AIMS™ EUV tool platform: aerial-image based qualification of EUV masks

Renzo Capelli, Martin Dietzel, Dirk Hellweg, Grizelda Kersteen, Ralf Gehrke, et al.

Renzo Capelli, Martin Dietzel, Dirk Hellweg, Grizelda Kersteen, Ralf Gehrke, Markus Bauer, "AIMS™ EUV tool platform: aerial-image based qualification of EUV masks," Proc. SPIE 10810, Photomask Technology 2018, 108100V (23 October 2018); doi: 10.1117/12.2501379

SPIE.

Event: SPIE Photomask Technology + Extreme Ultraviolet Lithography, 2018, Monterey, California, United States

AIMS™ EUV tool Platform: Aerial image based qualification of EUV masks

Renzo Capelli[1], Martin Dietzel[1], Dirk Hellweg[1], Grizelda Kersteen[1], Ralf Gehrke[1], Markus Bauer[2]

[1] Carl Zeiss SMT GmbH, Rudolf-Eber-Str. 2, 73447 Oberkochen, Germany

[2] Carl Zeiss SMT GmbH, Industriestr. 1, 64380 Roßdorf, Germany

ABSTRACT

With the EUV high volume manufacturing becoming reality and the closing gap of EUV mask infrastructure, EUV lithography is seeing or will shortly see the first production chips being fabricated with EUV. Pilot production in EUV HVM is most likely realized in a mix-and-match process with 193nm techniques. The degree of complexity introduced by the EUV lithographic process is transferred in parallel also to EUV mask: the combination of process sensitive 3D effects and material dependent EUV reflectivity make even the simplest EUV mask what the community is recognizing to be a very complex phase object. The qualification of such a complex piece of Infrastructure as the EUV mask is being addressed from many directions: defect review application is always more backed up by ancillary applications which aim at qualifying the printing behavior of the mask with the fundamental precondition of a full scanner emulation. ZEISS and the SUNY POLY SEMATECH EUVL Mask Infrastructure consortium have developed and commercialized the EUV aerial image metrology platform, the AIMS™ EUV platform, which fully addresses the industry requirements for EUV defectivity review. Additionally, this tool platform allows for mask qualification applications based on the employment of aerial image proven technology.

In this paper, the status and recent achievements of the AIMS™ EUV platform will be presented. Promoting the detailed exploration of the aerial image content potential for EUV process understanding and mask qualification, we will present recent results on a printability study of embedded EUV multilayer defects, along with providing further insights into the relevance of mask 3D effects.

Keywords: Mask metrology, AIMS™, Aerial image review, EUV, scanner emulation, defect review, EUV optics

1. INTRODUCTION

Having missed a few nodes of the ones for which EUV lithography was originally planned for, single exposure EUV lithography will have a few more opportunities for semiconductor manufacturing in high volume starting at the 7nm node. While the source power reaches the target operation value and the exposure tools improve their availability in a production environment in the wafer fab [1], the industry is now focusing on closing the gap on the remaining open items required for a fully operative infrastructure: from the wafer side, a viable resist solution and stochastics failures management are still thorough investigation. On the mask infrastructure side, production worthy solutions for an actinic patterned mask inspection tool and the mask pellicle are still being addressed. Despite the remaining gaps which still need commitment from semiconductor manufacturers and suppliers, EUV lithography has already been introduced in pilot production, and some layers are already produced using EUV exposure [2]. On the mask manufacturing side, zero defects blanks can be manufactured and also absorber defects are in limited numbers on high end masks [3]. Due to the complexity of 3D effects inherent to the EUV imaging process of standard masks with 70nm Ta based absorber, some private companies and research institutions are now investigating the solution space for the simplification of the EUV imaging process, e.g. by employment of thinner and chemically different absorber materials [4] which will also introduce benefits on the scanner side, above all an improvement of the process window. As we reported in recent contributions [5], the full scanner emulation capabilities provided by AIMS™ EUV can be employed by the mask shop for process optimization and full understanding of the complexity of the EUV imaging process: besides being used in production for defect review and repair verification, the AIMS™ EUV system is the perfect tool to qualify mask 3D effects and qualify production worthy process optimizations to minimize their impact.

In this paper the most evident advantages of AIMS™ EUV aerial image technology in the field of defect review and repair verification for EUV photomasks, as well as overall qualification of the aerial image formation and the EUV printing process, will be presented. Section 2 will give a short update on the status of the AIMS™ EUV production pipeline. Further studies on the complexity of the EUV imaging process related to mask 3D effects have also been performed by ZEISS with the AIMS™ EUV and the results will be presented in Section 3. In Section 4 a multi metrology qualification of the printing behavior of programmed multilayer defect will be presented.

Photomask Technology 2018, edited by Emily E. Gallagher, Jed H. Rankin, Proc. of SPIE Vol. 10810, 108100V · © 2018 SPIE · CCC code: 0277-786X/18/$18 · doi: 10.1117/12.2501379

2. AIMS™ EUV AS GOLD STANDARD FOR DEFECT REVIEW AND REPAIR VERIFICATION

The Aerial Image Measurement System (AIMS™) tools from ZEISS have been serving the semiconductor industry since 1993, when the first aerial image algorithm was developed in collaboration with IBM to work in a connection with a table top microscope. Since then, several systems generations have been introduced to the market in order to fulfill the mask shop need for mask defect review and repair verification applications. As for all AIMS™ systems, the AIMS™ EUV is employed within the back end of the line of a mask shop production environment in a closed loop with the ZEISS MeRiT® system for mask defect review and repair as shown in Figure 1. After being inspected by an inspection system, a mask is delivered to AIMS™ EUV along with a list of potential defective areas on the mask which could print as defect on the wafer and hinder the performance of the final chip product. The AIMS™ EUV defect review delivers the information on the printability of the defects under full scanner emulation conditions (wavelength, NA, illumination conditions, etc.): in order to correctly assess the printability of a defect, AIMS™ EUV collects all relevant information inherent the aerial image formation process the same way as the EUV NXE scanner does, providing therefore an exact preview of what the wafer will see as aerial image without the need of printing any wafer (develop the aerial image itself as a photographic plate).

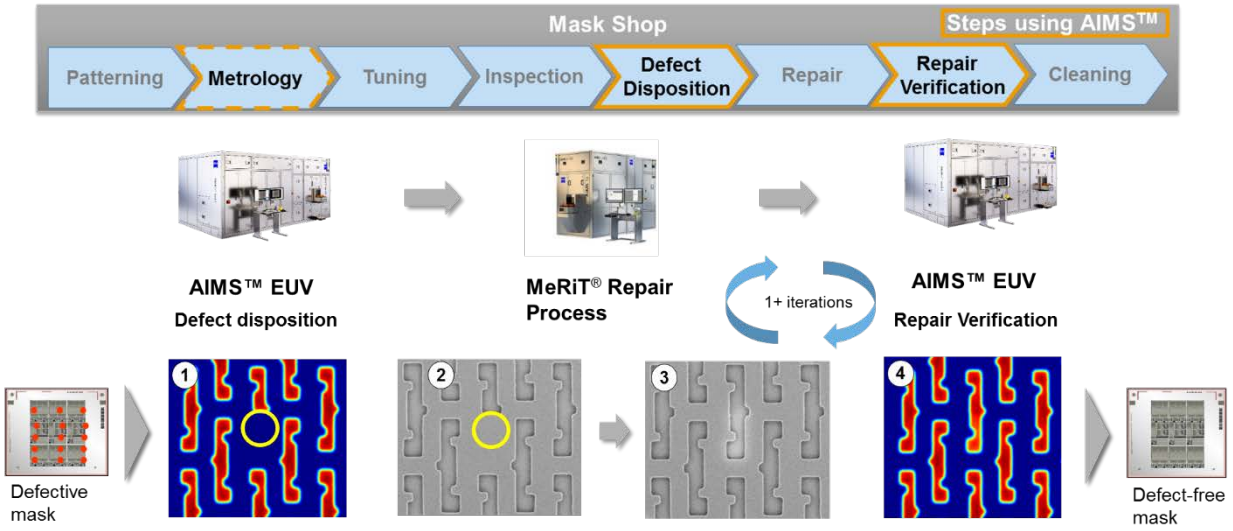

Figure 1: Exemplary mask production flow process. On the top line and in orange highlighted, the steps in which AIMS™ EUV is used. Bottom panel: 1. AIMS™ EUV aerial image of the defect. 2. Mask SEM image of the defective area. 3. Mask SEM image of the repaired area. 4. AIMS™ EUV aerial image of the repaired defect.

As reported in a recent contribution [6], the aerial image is the ideal place for a full mask qualification, for it measures the mask without any disturbance by photon/resist stochastics. Figure 2 shows a qualitative comparison between the wafer print and the aerial image of a dense contact holes array (structures are not the same): as it can be seen from the wafer print image, no clear separation between a mask error and wafer process can be made, given the noisy distribution of the feature size at wafer and the fact that a localization of an individual repaired defect with no anchor feature nearby becomes very complex. These factors contribute to a challenging repair verification process in the mask shop, as well as more complexity in the process optimization.

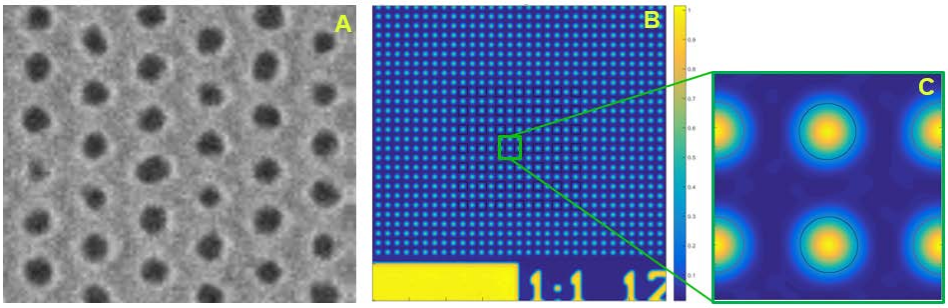

Figure 2: Feature regularity comparison between a CD SEM image from a wafer print (A) and the AIMS™ EUV aerial image of a dense contact holes array (B). On the right a zoom into the central region of the aerial image is shown (C). Note: aerial image and wafer print do not show the same mask field (structure).

On the other hand, the AIMS^{TM} EUV measures the mask without any disturbance by photon/resist stochastics, providing all information necessary to qualify the mask printing behavior with no impact from stochastics driven wafer processes. In the aerial image all mask optical effects are included, making possible to measure ΔCD and aerial image properties with high accuracy and repeatability and to provide a clean input for the repair process success and further process optimization.
In order to provide the industry with the competences of defect review and repair verification, as well as mask actinic qualification described above, the AIMS^{TM} EUV core capabilities as shown in Figure 3 are provided:

- Scanner equivalent illumination: the AIMS^{TM} EUV systems guarantees an equivalent image generation as on the NXE 33X0 and NXE34X0 EUV scanner systems. The information for the creation of the aerial image is collected by the projection optics the same way as it is on scanner, providing an equivalent image formation process which also supports different illumination schemes as available in exposure tools.
- Chief ray angle emulation: the AIMS^{TM} EUV illuminates the mask in one small spot, whereas the scanner slit illuminates the mask across the entire 104mm exposure field. Depending on the X position to be imaged on the mask, the angular distribution of EUV photons hitting the structure is different having the same polar 6 degree chief ray angle but different azimuthal component which introduces different shadowing across the mask X axis. AIMS^{TM} EUV can fully emulate this effect by the synchronized movement of the sigma and NA apertures.

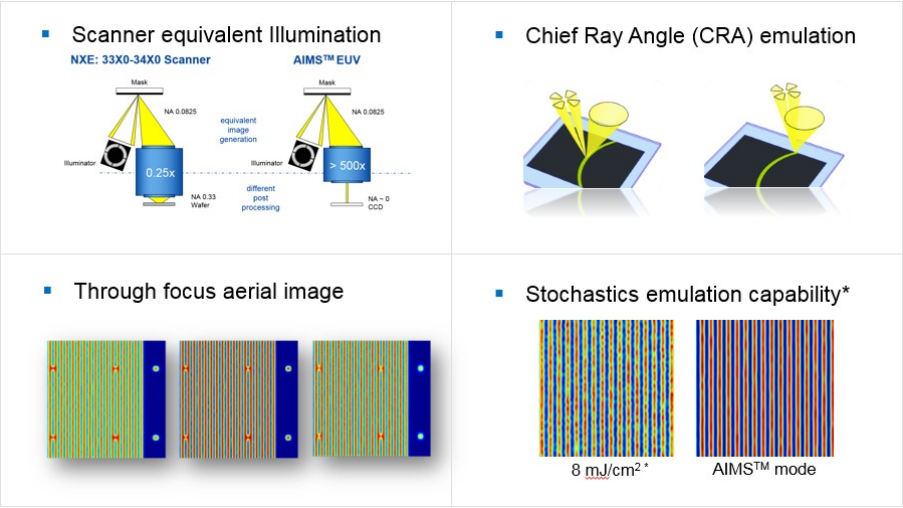

Figure 3: AIMS^{TM} EUV core capabilities for defect disposition and repair verification applications. See text for description.

- Through focus aerial image: the final product of AIMS^{TM} EUV is a focus stack of aerial images, i.e. one aerial image can be acquired for several focus planes, therefore allowing through focus defect disposition and process window optimization studies.
- Stochastics emulation: having the detailed knowledge of the AIMS^{TM} EUV system, we can provide an emulation of the dose seen by the wafer on the scanner, allowing the user to measure with the same photon number per area as used in wafer exposure and thereby introduce the photon shot noise component in the qualification of the mask printing process. The bottom right panel of Figure 3 shows an exemplary 2x2um field with 64nm L/S pattern on AIMS^{TM} EUV calibration mask, measured in Stochastics mode (left) and in normal defect review mode (right). In AIMS^{TM} defect review mode the stochastic variations are (almost) "switched off", allowing for most reliable defect characterization. In stochastics mode the photon noise contribution to e.g. LWR, local CDU or process-variation bands in hotspot analysis can be measured. The 8 mJ/cm^2 dose is the equivalent of a scanner dose of 40mJ/cm^2 in the aerial image with 20% resist absorption.

3. STATUS UPDATE FROM THE PRODUCTION PIPELINE

The AIMS^{TM} EUV first batch of tools built consist of a prototype system and three customer tools. As it was reported early 2018, the AIMS^{TM} EUV prototype tool achieved the last milestone of the development project in December 2017 and it now serves the purposes of EMI members access demonstration, platform software and hardware development, training for customer operators and ZEISS service personnel, as well as the development of new aerial imaged based applications. To describe the tool availability during the afore mentioned EMI access campaigns, the graph in Figure 4 shows the recorded productive time for each measurement slot: after the first campaigns in which the level of machine automation was still limited and control software features were still being developed, the platform demonstrates very good availability and performance quality very well comparable to customer tools. As it has been reported in [7], the first AIMS^{TM} EUV customer tool has been handed over to Intel mask shop for insertion into production, following successful integration and final acceptance.

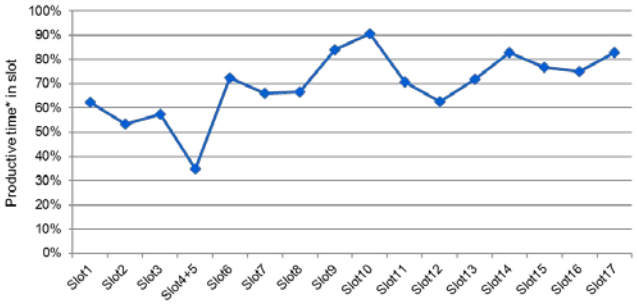

Figure 4: AIMS^{TM} EUV prototype productive time as measured during EMI customer access campaigns. Productive time is measured within timeframe of the CAS campaign only, neglecting e.g. preparation efforts to bring the tool to measurement state. Productive time is not measured according to SEMI E-10 standard for uptime.

The second and third customer tools also successfully passed factory acceptance demonstrating excellent imaging performance and tool stability. These systems are now in integration at two different customer sites and after going through hardware integration and start-up phase, their performance will be tested within final acceptance and later they will be handed over to customers for insertion into the production flow.

4. AIMS^{TM} EUV QUALIFICATION OF MASK 3D EFFECTS: PATTERN SHIFT THROUGH FOCUS

Over the recent years the AIMS^{TM} EUV platform has been employed by ZEISS and the EMI members for the detailed study of EUV imaging topics [e.g. 7]. To continue on the series, the mask 3D effect given by the pattern shift through focus typical of EUV imaging process will be described and quantified in this chapter. A confirmation of the relative importance of this effects for the overall EUV imaging budget can be noticed from the number of investigations that recently appeared in the literature [8] which try to quantify this effect as a function of typical mask and lithographic process parameters (e.g. illumination conditions, structure pitch, absorber height). In fact, the impact of pattern shift through focus on EUV imaging is already being qualified with 0.55 NA [9].

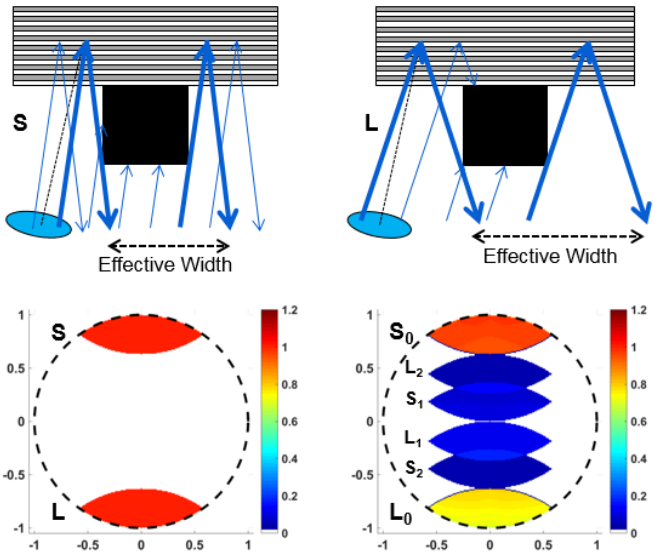

Figure 5: Graphical description of the origin for the telecentricity effect generated in the aerial image. Top row: light rays from the entrance pupil hit the mask with a narrow spectrum of incidence angles distributed around 6 deg. The indices S and L refer to Smaller and Larger angle of incidence with respect to the nominal chief ray angle of 6 deg (object side). Bottom row: on the left an ideal dipole illumination pupil is displayed (S and L refer to the angles as in the top row). Right: Exit pupil, in which the diffraction orders coming from the two poles collected into the NA are displayed with different intensities and coded 0 to 2.

Figure 5 attempts at graphically explaining the cause of pattern shift through focus, i.e. the telecentricity effect. Because of the reflective nature of EUV mask, the at mask ingoing and outgoing ray bundles have to be separated by a minimum angle; in order to meet this requirement, at 0.33NA imaging the mask is illuminated with EUV photons being distributed about a chief ray angle at object (CRAO) of 6 degrees. If α is the half angular range of the EUV photons going through the entrance pupil, the two extremes angles which are used in the imaging process are $6 \pm \alpha$, respectively labeled with L (large) and S (small) in Figure 5. The second component to be considered in the formation

of the telecentricity effect is the angular dependence of the EUV reflectivity by a Bragg multi-layer such as a EUV mask; a tilt of few degrees of the incident angle can return a significantly different reflectivity of the same mask sample. This reflectivity asymmetry, in addition to the main effect introduced by the geometric imbalance in the over casted shadow produced by the absorber stack, introduces a shift of the pattern placement, which is a relevant effect for EUV lithography which needs to be quantified and biased for on the mask. By employing an exemplary dipole illumination as the one shown in the bottom panel of Figure 5, in which the two poles are separated by a few degrees, the same index diffraction orders reflected from the mask will have a different intensity whether they are generated from the L or S pole.

Previous attempts for quantifying the pattern shift through focus for a dense contact holes array surrounded by anchor lines structures have been reported as measured on the SHARP tool [10], in which only an upper limit to this quantity could be set. A similar measurement campaign was run on the AIMS^{TM} EUV system in order to quantify the amount of pattern shift through focus as a function of several imaging parameters such as azimuthal position within the scanner arc slit, illumination pupil and structure pitch and orientation. In order to measure the pattern placement, a threshold is calculated for the best focal position and used to calculate the pattern position to be center point between the two intersections of the intensity profile with the threshold level.

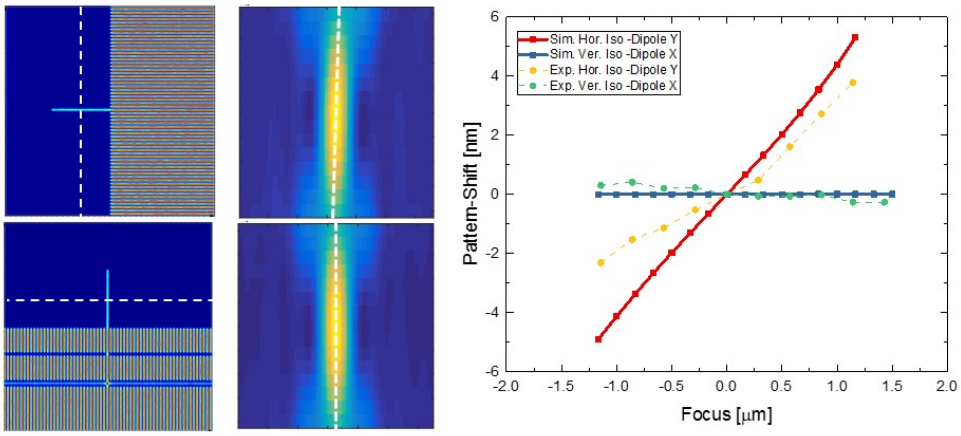

Figure 6: Left column: AIMS^{TM} EUV aerial image of a dense lines and spaces array (64nm at mask) in which an isolated feature with same nominal CD is within the same field of view. The white dashed line in each plot shows the cutline used for the pattern shift through focus analysis. Center column: 1D intensity profiles (intensity per pixel) along the cutline shown in the left column aerial images (~8μm long). On the Y axis are the 25 different focus levels between ±2 μm measured within the focus stack. Right: comparison between simulation and measurement results. For the extreme focus levels a CD could not be measured as the intensity profile was below threshold level.

The first results are presented in Figure 6, in which the pattern shift for isolated horizontal and vertical spaces is measured for several focus positions in the center of the mask, and compared to expectation values from rigorous simulations. Due to symmetry around oblique CRA (6 deg), a significant pattern-shift through focus is to be expected for horizontal structures, whereas for the vertical counterparts this effect should be negligible. AIMS^{TM} EUV measurements qualify the fundamental differences of horizontal and vertical structures due to oblique CRA, confirming the trends also observed in simulation (Figure 6, right panel). The second imaging parameter which was investigated in the framework of the pattern shift through focus qualification is the X position within the scanner field. The aerial images of an isolated horizontal and vertical space were acquired for 10 focus positions in the center and two mid-edge positions (±26 mm) across the scanner arc and the pattern shift through focus compared for the structure orientation and scanner arc position. From the results in Figure 7 it can be seen that the rotation of the azimuthal component of the CRAO has no significant impact on the patterns shift through focus of the horizontal lines, as all three lines follow the same trend both qualitatively and quantitatively. On the other hand, due to the asymmetry introduced by the CRAO rotation, the pattern placement through focus as measured for vertical features shows a strong dependence on the mask position, displaying opposite behaviors in extreme cases; in the center of the mask a negligible pattern shift is observed, whereas at the two side positions an increasing (decreasing) pattern shift is measured for negative (positive) scanner arc X position, with both curves showing well comparable total ranges. Further, the dependence of the pattern shift through focus on the illumination pupil settings was qualified; the same measurements of an isolated horizontal space were acquired with NXE:33X0 quasi-conventional and dipole-Y settings, the imaging pupils as measured by the AIMS^{TM} EUV system being shown in the right panels of Figure 8. The technique employed to extract information from the aerial images as for the pattern placement through focus was the same used for the qualification of the previous process parameters: the AIMS^{TM} EUV measurements show, that the pattern shift through focus heavily depends on the shape of the illumination pupil (see left panel of Figure 8). As a last imaging parameter to be investigated for pattern placement shift through focus, the structure pitch was selected: the same aerial images measured with the dipole-Y pupil of an horizontal isolated space as used for previous measurements have been

selected, for two different pitches (isolated and dense, i.e. 1 to 1) can be found for the same nominal CD at mask within the same field of view (see left panel in Figure 9). The impact of the structure pitch on the trends observed in the measurements of the pattern shift through focus of horizontal spaces (and lines) can be seen in the two graphs reported in Figure 9. The plot for the isolated space resembles the ones already presented in Figure 7, and it is greatly different from the trends measured for the dense lines and spaces (yellow region of interest in the aerial image of Figure 9): for this 1 to 1 structure pitch, no significant pattern shift is observed for negative mask positions, whereas it increases exponentially going through the center towards the positive X edge of the mask.

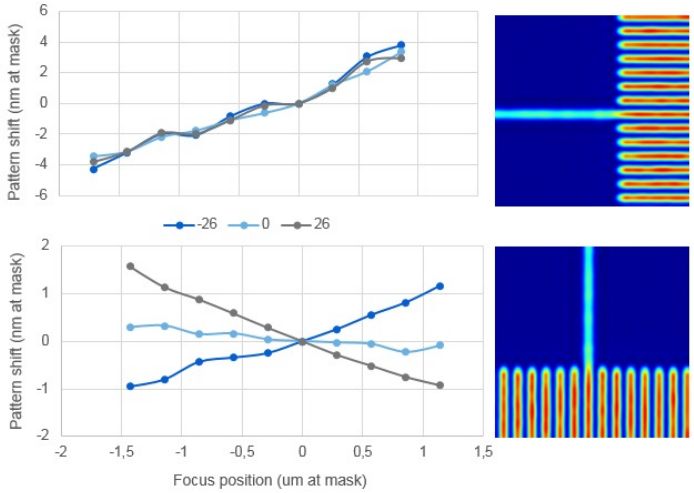

Figure 7: AIMS^{TM} EUV qualification of pattern shift through focus dependence on feature orientation for the isolated space features shown in the aerial image snapshots on the right. The pattern shift through focus measured from the aerial image stack is plotted in nm at mask level against the focus position for different mask X positions given in mm.

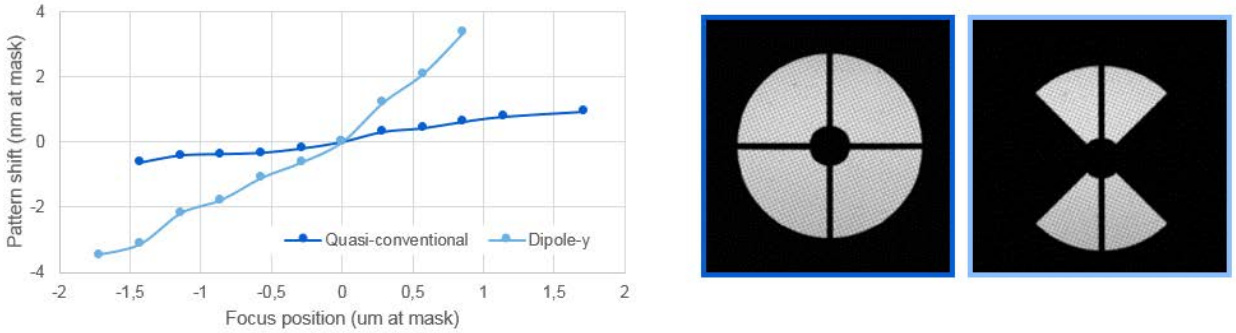

Figure 8: AIMS^{TM} EUV qualification of pattern shift through focus dependence on the illumination scheme for the illumination pupils shown on the right (respectively quasi-conventional and dipole-Y). The pattern is the same isolated horizontal space of Figure 7, for which the shift through focus measured from the aerial image stack is plotted in nm at mask level against the focus position for the two different illumination pupils.

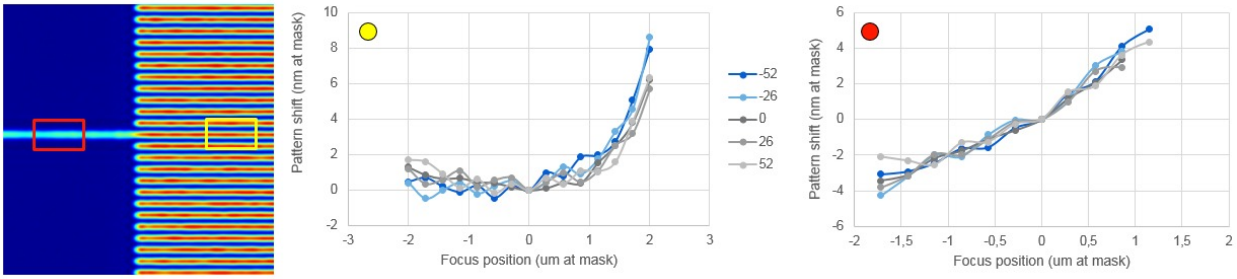

Figure 9: AIMS^{TM} EUV qualification of pattern shift through focus dependence on structure pitch, i.e. isolated and dense. A focus stack of the same mask field has been collected with the five different scanner X positions (in mm) as reported in the plots legend. The red and yellow circles in the pattern shift plots refer to the colored ROIs in the aerial image (red and yellow for isolated and dense feature respectively).

The results of this section clearly show the complexity of the telecentricity effect as for the impact it has on the EUV imaging process. The strong dependencies on several process parameters will have to be taken into account by mask architects in order to be biased and/or corrected for already on the mask. In order to deliver the perfect mask for EUV

production, a qualification of the full mask printing behavior is necessary and a benchmarking of simulations results with actinic measurements is needed to establish and optimize production processes. As shown in this section, the pattern shift through focus requires the high quality full scanner emulation provided by the AIMS™ EUV system: more generally, the AIMS™ EUV platform provides the means for a full qualification of the mask 3D effects dependence on process parameters.

5. AIMS™ EUV PRINTING ASSESSMENT OF PROGRAMMED MULTILAYER DEFECTS

Previous studies of multi-layer defect printability with AIMS™ EUV, as well as the comparison between wafer prints and AIMS™ EUV aerial image were performed in collaboration with Globalfoundries in the framework of the customer access program to the AIMS™ EUV prototype [11]. In this contribution, we report results from a multi metrology study of exemplary native multi-layer defects as detected by the actinic blank inspection tool on the PASHAL EUV mask. The full study was done on a sample of 146 multi-layer defects within a collaboration between Imec, AMTC and ZEISS in the framework of the 7nm technology (SeNaTe) European project [12]. Figure 10 shows a qualitative comparison between the NXE:3300 scanner wafer print of six exemplary native multi-layer defects and the aerial image acquired by AIMS™ EUV employing full scanner emulation. Within an area of 8 by 8 um, corresponding to the full field of view of the AIMS™ EUV camera, eight 'T' and 'L' shaped structures can be observed both on the wafer print and in the aerial image. These anchor structures were printed on the mask after the blank inspection identified the position of the native multi-layer defects, in order for these defects to be measured in the center of this frame.

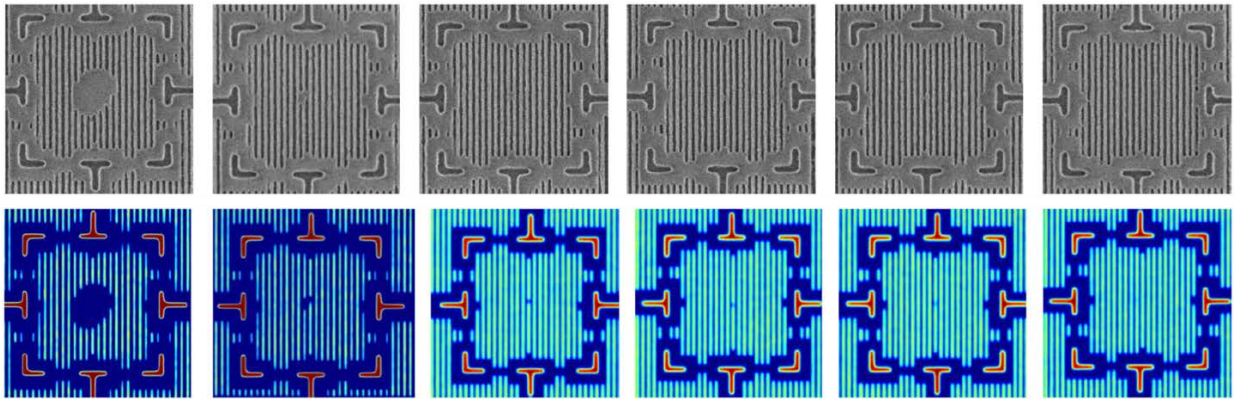

Figure 10: Qualitative comparison between wafer prints of PASHAL exemplary multi-layer defects and the AIMS™ EUV aerial image of the same mask fields. According to the design and ABI inspection results, the defect is expected in the center of the bright red frame markers (wafer exposed with NXE:3300 scanner, data courtesy of Imec).

Figure 10 shows a remarkably good agreement between the defects printability as measured in the aerial image and as observed on wafer prints over the range of printing impact. Employing the capability of measuring through focus provided by AIMS™ EUV, it can be seen that this good correlation extends to defocus conditions within the process window. Two of the 146 defects found on the mask were investigated in greater details and the results are shown in this work. Figure 11 presents a multi metrology printability assessment of one specific multi-layer defect: on the left panel, the mask SEM image, in which the defect frame structures are well visible but a defect is not detected at its center. AFM inspection was able to measure this specific defect and the profile along the trench can be seen in the mid left panel of Figure 11, indicating the presence of a ~4nm high bump on top of the multi-layer reflective surface.

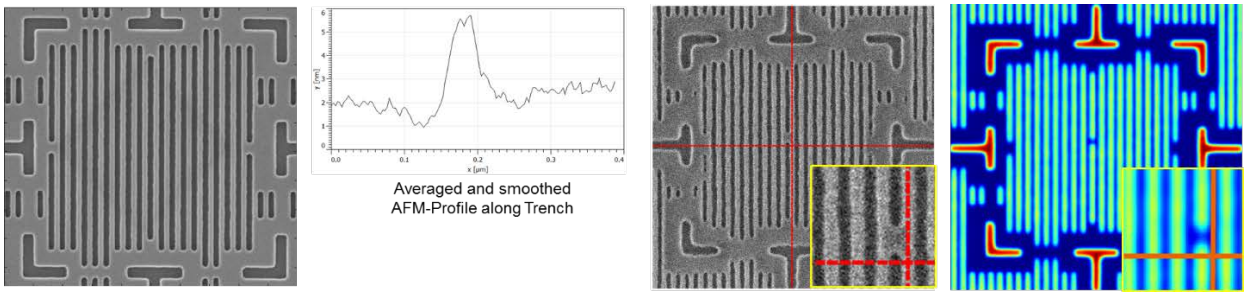

Figure 11: Multi-metrology printability assessment of buried blank defect. From left to right: Mask SEM image, in which a defect is not visible; AFM profile (courtesy of ZEISS SMT), averaged and smooth along the trench, in which a ~4nm high bump is visible; wafer print of the same mask field, with the defect clearly printing and resulting in a large bridging of two adjacent lines; AIMS™ EUV image of the same defective area, where the defect is visible in the center. Two inlets are included in the two images on the right, showing the position of the printing defect as printed by the scanner and measured by AIMS™ EUV compared to the position expected from ABI.

The most important result come from the comparison of the wafer print and AIMS™ EUV aerial image: in both images, the center of gravity of the defect is measured consistently at about 1 half-pitch distance from the expected position (measured with ABI). This example demonstrates the additional value of actinic review via AIMS™ EUV: the deviation of the actual defect position from the expected position can be quantified, and the printability assessment delivers the information which is the most accurate and closest to the scanner wafer printing result. The full qualification of the printing behavior is only possible via the analysis of the AIMS™ EUV aerial image: for this specific defect case, what was expected to be buried underneath the absorber, results in printing as a bridging defect.
As a second example, a case of defect detection underneath the absorber is shown in Figure 12. The left two panels show the aerial image full field of view with the multi-layer defect expected in the center of the bright frame structures, as well as a zoom into the image center, centered on the defect position. Within the zoomed in aerial image, a dark spot is visible at the expected defect position: follow up AFM review shows the presence of a ~2.5nm deep pit, which can measured by AIMS™ EUV with a larger than 25% contrast. The Fresnel reflection from the absorber surface calculated for a TaN based absorber would be very small when compared with the signal measured in the aerial image. The observed multi-layer defect and mask speckle seen within the AIMS™ EUV images in the un-patterned areas is therefore dominantly from light amplitude that has transmitted the absorber, is reflected in the multilayer, and has transmitted the absorber a second time.

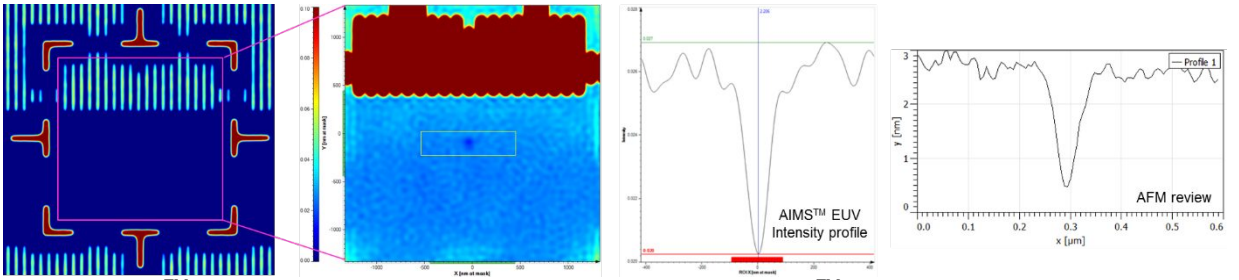

Figure 12: AIMS™ EUV defect detection below absorber. From left to right: AIMS™ EUV aerial image of the defective mask field; zoom into the aerial image with a different contrast and color scale used to highlight the intensity drop caused by the defects underneath the absorber; intensity profile of the defect as measured in the aerial image; AFM profile of the same defect (courtesy of ZEISS SMT).

Also when underneath the absorber, a ML-defect is visible and its imaging impact can be quantified. The system is extremely sensitive to the mask material compositions and its changes in optical constants. This sensitivity opens a range of diverse applications that the platform can support beyond defect review and repair verification: qualification of phase shift masks, material qualification such as thinner absorbers (Co, Ni) and their imaging impacts, pattern shift review, black border qualification and process development. Concluding, the AIMS™ EUV platform capabilities go well beyond defect disposition and review.

6. SUMMARY AND OUTLOOK

In this paper, the most recent achievements and measurement results of the AIMS™ EUV platform have been presented. This actinic metrology platform provides all capabilities for a complete defect review and EUV mask qualification. In specific, we have shown that:

- The first commercial tool has been handed over to Intel mask shop in production following the successful tool integration and final acceptance qualification.
- Two more customer tools successfully passed factory acceptance with excellent performance.
- AIMS™ EUV capabilities provides all the means for a full ‘scanner aware’ qualification of the mask 3D effects dependence on process parameters.
- A good correlation to wafer prints over the range of printing impact of programmed multi-layer defects has been shown on PASHAL mask.
- AIMS™ EUV additional values demonstrated for exemplary multi-layer defects. The platform is extremely sensitive to material optical properties and can detect and qualify imaging impact of defects buried underneath absorber. Moreover, a measurement of the deviation of the actual defective position from the expected position given by an actinic inspection tool can be qualified with the ‘scanner aware’ actinic aerial imaging technology provided by AIMS™ EUV.

The capabilities of the AIMS™ EUV platform go well beyond defect disposition and review: platform extensions can offer both hardware (High NA upgrade, pellicle upgrade) and software solutions (AIMS™ AutoAnalysis EUV, aerial image content analysis).

7. ACKNOWLEDGEMENTS

The authors would like to thank SUNY POLY SEMATECH and the EMI members for their support and contributions to the AIMS™ EUV project. ZEISS thanks IMEC for providing the wafer print images of the PASHAL mask. This PASHAL mask was a collaboration between imec, AMTC and Zeiss, under EU project "ECSEL JU 662338 SeNaTe".

8. REFERENCES

[1] M. Mastenbroek, 'NXE:3400B scanner, EUV volume manufacturing for 7nm node lithography and beyond', Proc. SPIE Vol. 10809, 10809XX, 2018.
[2] https://www.eetimes.com/document.asp?doc_id=1333827&page_number=1
[3] B. Kim, P. Buck, P. Morgan, T. Scherübl, T. Onoue, Panel discussion BACUS Photomasks Technology and EUV Lithography Conference 2018, Monterey, CA, USA.
[4] V. Philipsen at al., 'Novel EUV mask absorber evaluation in support of next generation EUV imaging', Proc. SPIE Vol. 10810, 10810XX, 2018.
[5] D. Hellweg et al., 'Actinic Review of EUV masks: Challenges and achievements in delivering the perfect mask for EUV production', Proc. SPIE Vol. 10451, 104510J, 2017.
[6] R. Capelli et al., 'Aerial image based metrology of EUV masks: recent achievements, status and outlook for the AIMS™ EUV platform', Proc. SPIE Vol. 10583, 1058311, 2018.
[7] Chen et al., 'Evaluation of EUV mask impacts on wafer line-edge roughness using aerial and SEM image analyses', Proc. SPIE Vol. 10583, 105830J, 2018.
[8] E. van Setten et al., 'High-NA EUV lithography: the next step in EUV imaging', Proc. SPIE Vol. 10809, 2018.
[9] V. Wiaux et al., 'Mask 3D effects experimental measurements with 0.55 NA anamorphic imaging', Proc. SPIE Vol. 10809, 2018.
[10] O. Wood et al., 'Measurement of through-focus EUV pattern shifts using the SHARP actinic microscope', Proc. SPIE Vol. 10450, 1450E, 2017.
[11] E. Verduijn et al., 'Printability and actinic AIMS review of programmed mask blank defects', Proc. SPIE Vol. 10143, 101430K, 2017.
[12] R. Jonckheere et al., 'Blank defect coverage budget for 16nm half-pitch single EUV exposure', Proc. SPIE Vol. 10807, 2018.